

All-optical control of the spin state in the NV^- -center in diamond

Florian Hilser and Guido Burkard

Department of Physics, University of Konstanz, D-78457 Konstanz, Germany

We describe an all-optical scheme for spin manipulation in the ground-state triplet of the negatively charged nitrogen-vacancy (NV) center in diamond. Virtual optical excitation from the 3A_2 ground state into the 3E excited state allows for spin rotations by virtue of the spin-spin interaction in the two-fold orbitally degenerate excited state. We derive an effective Hamiltonian for optically induced spin-flip transitions within the ground state spin triplet due to off-resonant optical pumping. Furthermore, we investigate the spin qubit formed by the Zeeman sub-levels with spin projection $m_S = 0$ and $m_S = -1$ along the NV axis around the ground state level anticrossing with regard to full optical control of the electron spin.

I. INTRODUCTION

Nitrogen-vacancy (NV) centers in diamond have attracted much attention in research related to quantum computation¹ due to their key advantages, such as high stability and long spin coherence times²⁻⁴ up to room temperature and beyond⁵. The spin coherence time can be increased further by isotopic engineering⁶ since only the ^{13}C carbon atoms have non-zero nuclear spin, thus contributing to spin decoherence due to hyperfine coupling. Under resonant optical excitation the NV^- center exhibits a strong and highly stable zero phonon line at 1.945 eV⁷ with an excited state lifetime of about 12 ns⁸. Electron spin resonance analysis of the center has shown that both ground state and excited state are spin triplets, which implies that there is an even number of active electrons involved. The ground state levels with spin projection $m_S = 0$ and $m_S = -1$ along the NV axis become degenerate in a magnetic field of about 1025 G. Optical pumping causes a spin polarization of the ground state⁹⁻¹¹ that can be attributed to a spin-orbit induced intersystem crossing with an intermediate singlet state¹². When the zero field splitting is larger than the optical linewidth, repeated optical excitation leads to a spin selective steady state population in the lowest $m_S = 0$ level of the ground state, generating a non-Boltzmann steady state spin alignment and mixing of spin states¹⁸, so the spin of the ground state can be both initialized and read out optically¹⁷.

The standard procedure for spin manipulation in the ground state triplet involves an oscillatory (radio-frequency) magnetic field that gives rise to electron spin resonance. In this paper, we describe an alternative method for full spin control without rf-fields, based entirely on optical transitions. All-optical spin manipulation of NV centers could allow for fast operations with high spatial resolution. In semiconductor quantum dots, picosecond optical control of single electron spins has been achieved^{13,14}. Optically induced spin rotations in a single NV center in diamond have been demonstrated using off-resonant laser excitation¹⁵. This type of spin control relies on the optical Stark effect, i.e., the shift in energy levels induced by an applied optical field. Here, we describe an extension of this scheme which also allows for

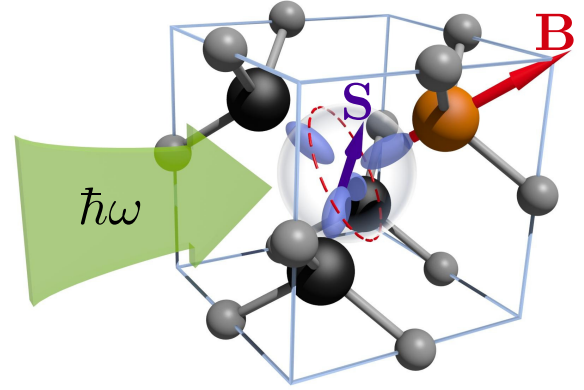


Figure 1. NV-center in diamond with equivalent sp^3 -hybridized dangling bonds (blue) σ_i ($i = 1, 2, 3$) from the surrounding carbon atoms (black) and σ_N from the substitutional nitrogen atom (orange) overlapping within the vacancy (center). The NV-axis (long red arrow) defines the z -axis of the coordinate system and, due to the zero field splitting determines the quantization axis of the electron spin. The magnetic field B is applied along the NV-axis.

transitions between the three ground state levels, similar to existing schemes for coherent population trapping¹⁶.

II. MODEL

To model optical spin rotations in an individual NV-center in diamond, we start from the commonly used description that fundamentally involves a total number of six electrons, but can be reduced to an effective two-electron^{12,19,20} or, equivalently, two-hole model²¹. The four relevant single-electron orbitals a_1 , a_2 , e_x , and e_y can be obtained by projecting the sp^3 -hybridized dangling bonds $\sigma_{1,2,3}$ of the carbon atoms and σ_N of the nitrogen atom (see Fig. 1) onto the irreducible representations of the C_{3v} symmetry group of the NV center²¹. The electron configurations for the ground and first ex-

cited state are obtained as follows: In the ground state (e^2) configuration, the lower-energy $a_{1,2}$ orbitals are completely filled with two electrons each, while the e_x and e_y contain one electron each. The two-fold degenerate excited state configuration (ae) is obtained by promoting another electron from a_1 to e_x or e_y . Due to the Coulomb interaction between the two electrons, the spin triplet lies lowest in energy and forms the ground state $e^2(T)$, transforming according to the representation A_2 of C_{3v} ²¹. Electric dipole transitions connect this triplet to the excited state spin triplet $ea(T)$, transforming according to the E representation. The two-fold orbital and three-fold spin degeneracies give rise to a total of six states in $ea(T)$, compared to three states in $e^2(T)$. The spin singlet states will not be of direct importance for our discussion, and are left out of our model. The entire state space for our model is thus nine-dimensional.

A. Ground state

The Hamiltonian of the ground state spin triplet in the basis $\{^3A_{2-}, ^3A_{20}, ^3A_{2+}\} = \{|-1\rangle, |0\rangle, |+1\rangle\}$ is

$$H_{\text{gs}} = \begin{pmatrix} D_{\text{gs}} - g_{\text{gs}}\mu_B B & 0 & 0 \\ 0 & 0 & 0 \\ 0 & 0 & D_{\text{gs}} + g_{\text{gs}}\mu_B B \end{pmatrix}, \quad (1)$$

$$H_{\text{es}} = \begin{pmatrix} D_{\text{es}}/3 + \Delta + l_z & g_{\text{es}}\mu_B B & 0 & 0 & \delta_x & -i\delta_y \\ g_{\text{es}}\mu_B B & D_{\text{es}}/3 - \Delta + l_z & 0 & 0 & i\delta_y & -\delta_x \\ 0 & 0 & -2D_{\text{es}}/3 + \delta_x & \delta_y & 0 & \Delta'' \\ 0 & 0 & \delta_y & -2D_{\text{es}}/3 - \delta_x & i\Delta'' & 0 \\ \delta_x & -i\delta_y & 0 & -i\Delta'' & D_{\text{es}}/3 - l_z & -g_{\text{es}}\mu_B B \\ i\delta_y & -\delta_x & \Delta'' & 0 & -g_{\text{es}}\mu_B B & D_{\text{es}}/3 - l_z \end{pmatrix}, \quad (2)$$

where l_z is the axial spin-orbit splitting, and $D_{\text{es}} = -\frac{3}{4}D_{zz}$ and $\Delta = \frac{1}{2}D_{x^2-y^2}$ are the well-known spin-spin interactions¹⁹. Experimentally, it was found that $l_z = 5.3$ GHz, $D_{\text{es}} = 1.42$ GHz and $\Delta = 1.55$ GHz²⁵. The Landé factors of ground and excited state were found to be equal²⁶⁻²⁸, $g_{\text{gs}} \simeq g_{\text{es}} \simeq 2.01 = g$. The energy gap E_g is defined as the difference between the $E_{1,2}$ excited states and the $m_S = \pm 1$ ground states at $B = 0$. The dependence of the ground- and excited state levels on B is shown in Fig. 2.

Since electric dipole transitions are spin-conserving, our all-optical spin control scheme requires a spin non-conserving mechanism in the excited state. The longitudinal spin-orbit interaction term l_z only leads to an additional energy splitting between states with different spin projections and cannot flip the spin. It was speculated that the transversal part of the spin-orbit interaction can lead to spin flips^{23,24}, but it has recently turned out that it can only connect orbital states belonging to different irreducible representations²¹. However, the transversal

where B denotes an external magnetic field aligned with the NV -axis, g_{gs} the Landé g-factor, and μ_B the Bohr magneton. Around the ground-state level anticrossing (LAC), we can split the Zeeman energy into a term that compensates the ground state zero field splitting and an additional variation, $g\mu_B B = D_{\text{gs}} + g\mu_B \delta B$. The zero field splitting $D_{\text{gs}} = 2.88$ GHz²² is caused by the reduction of the symmetry in spin space to C_{3v} due to the crystal field. The absence of orbital degeneracy in the ground state triplet implies that strain and spin-orbit interaction have very little effect on the ground state.

Here, we have neglected the effect of the hyperfine coupling to the nuclear spins of the intrinsic nitrogen atom and surrounding ^{13}C atoms. If necessary, the nuclear spin state could be prepared optically.

B. Excited state

At low temperatures, the excited state fine structure can be understood to a large extent from strain and spin-spin interactions. In the basis of spin-orbit states with full symmetry, described by the C_{3v} double group including spin²¹, $\{A_1, A_2, E_X, E_Y, E_1, E_2\}$ the excited-state Hamiltonian matrix is

component $\Delta'' \simeq 0.2$ GHz of the spin-spin interaction allows for the non-spin-conserving transitions between the E and E' states, explaining the experimentally observed transitions²¹.

The components δ_x and δ_y of the non-axial strain can be written in polar coordinates, $\delta_{\perp}^2 = \delta_x^2 + \delta_y^2$ and $2\beta = \arctan(\delta_y/\delta_x)$. Here, β was defined such that it corresponds to the angle between the symmetry axis of strain eigenstates $e'_x(\delta_x, \delta_y)$ and the symmetry axis of the unperturbed e_x -orbital.

C. Electric dipole transitions

We assume the system to be optically driven with a radiation field at fixed frequency ω near E_g , therefore it is convenient to describe the excited states in a corotating frame, while keeping the ground states fixed. We then work in the rotating wave approximation where counter-rotating terms with frequency $E_g + \omega$ are neglected. This

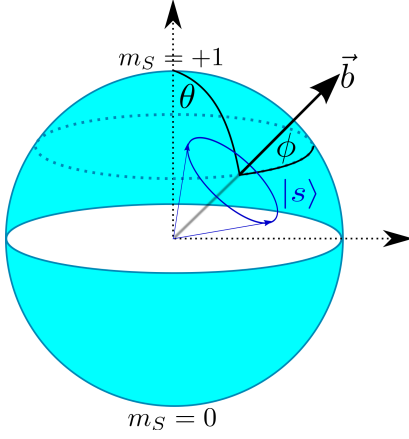


Figure 3. The state $|s\rangle$ of the ground state spin qubit in the $m_S = 0, -1$ subspace can be represented as a vector on the Bloch sphere where the two poles represent the two Zeeman-split eigenstates $|m_S = 0\rangle$ and $|m_S = -1\rangle$. The vector \mathbf{b} denotes the effective magnetic field acting on this pseudo-spin $1/2$, with spherical angles θ and ϕ .

B. Rotation axis

We focus on the transition between the $m_S = -1$ and $m_S = 0$ ground state spin levels. This two-level system can be split off from the $m_S = +1$ state³⁰, in the regime $g\mu_B|\delta B| \lesssim 2D_{\text{gs}}$. In this case the dynamics is described by the 2×2 Hamiltonian

$$\tilde{H} = \begin{pmatrix} \tilde{H}_{11} & \tilde{H}_{12} \\ \tilde{H}_{21} & \tilde{H}_{22} \end{pmatrix} = b_0 \mathbb{1} + \mathbf{b} \cdot \boldsymbol{\sigma} \quad (13)$$

where the effective (pseudo-) magnetic field has components,

$$b_x = \frac{1}{2} (\tilde{H}_{12} + \tilde{H}_{21}) = b_{\perp} \cos \phi, \quad (14)$$

$$b_y = \frac{1}{2i} (\tilde{H}_{12} - \tilde{H}_{21}) = b_{\perp} \sin \phi, \quad (15)$$

$$b_z = \frac{1}{2} (\tilde{H}_{11} - \tilde{H}_{22}), \quad (16)$$

and $b_0 = \tilde{H}_{11} + \tilde{H}_{22}$. The dynamics within this two-dimensional subspace can be visualized using a Bloch sphere picture, as shown in Fig. 3. Optical driving results in a rotation of the state vector about an axis \mathbf{b} with polar angle (axial orientation) θ and azimuthal angle (non-axial orientation) ϕ . The transversal part $b_{\perp} = |\tilde{H}_{12}| = \sqrt{b_x^2 + b_y^2} = b \sin \theta$ of the effective field provides for effective spin-flip transitions while b_z accounts for the effective (AC Stark) splitting between the two levels (around the LAC). The term $\propto \mathbb{1}$ in Eq. (13) can be omitted since it merely leads to a global phase. The precession frequency is given by

$$b = \sqrt{b_{\perp}^2 + b_z^2} = \sqrt{1 + \cot^2 \theta} |b_{\perp}|. \quad (17)$$

Spin flips can be implemented as rotation about an axis within the equatorial plane of the Bloch sphere (Fig. 3) which corresponds to $\theta = \frac{\pi}{2}$ and thus $b = b_{\perp}$.

IV. RESULTS

A. Unstrained NV center

In the case of vanishing strain ($\delta_{\perp} = 0$) we obtain a simple analytical result for the transversal component of the qubit rotation axis, with magnitude,

$$b_{\perp} = \Delta'' \epsilon^2 \left| \frac{1}{\delta\omega(\delta\omega + D_{\text{es}} + l_z + D_{\text{gs}} + g\mu_B\delta B)} + \frac{1}{(\delta\omega - g\mu_B\delta B)(\delta\omega - D_{\text{es}} + l_z + D_{\text{gs}})} \right| + O(\Delta''^2), \quad (18)$$

which is proportional to the intensity ϵ^2 of the optical driving field and the transversal spin-spin coupling Δ'' in the excited state. The azimuthal angle of the rotation axis is determined by the optical polarization angle α ,

$$\phi = -2\alpha \quad (19)$$

where the factor of 2 reflects the double group character of spin representation. The polar angle θ of the rotation axis is independent of α and for small $g\mu_B\delta B$ even independent of the driving field strength ϵ . The residual Zeeman splitting is limited by the hyperfine LAC of about 2 MHz³³, and therefore for an optical coupling $\epsilon \gtrsim 100$ MHz we can always find pairs of parameters $(\delta B, \delta\omega)$ that fulfill the condition $\theta = \pi/2$.

In the limit of large detuning, i.e., when $\delta\omega$ dominates all other energies in the denominators of Eq. (18), we can approximate the transverse component of the effective field as

$$b_{\perp} \simeq 2\Delta'' \frac{\epsilon^2}{\delta\omega^2}. \quad (20)$$

B. Effect of strain

We now include the effect of strain in the diamond crystal into our discussion. For moderate strain $\delta_{x,y} \ll 2l_z \approx 10$ GHz, the $A_{1,2}$ levels of the excited state are largely separated from the $E_{1,2}$ levels, and thus the strain-induced mixing of $A_{1,2}$ states and $E_{1,2}$ states can be neglected in lowest order. The main effect of moderate strain is thus a shift of the resonances in Eq. (18) by $\pm\delta_{\perp} = \pm\sqrt{\delta_x^2 + \delta_y^2}$, lifting the degeneracy of E_x and E_y levels. Though strain does not directly mix states with different spin projections, this shift reduces the energetic separation between coupled E and E' levels and therefore strongly enhances the efficiency of spin-flip-transitions. In Fig. 4, we plot suitable pairs of parameter values for the detuning $\delta\omega$ (near resonant driving) and Zeeman

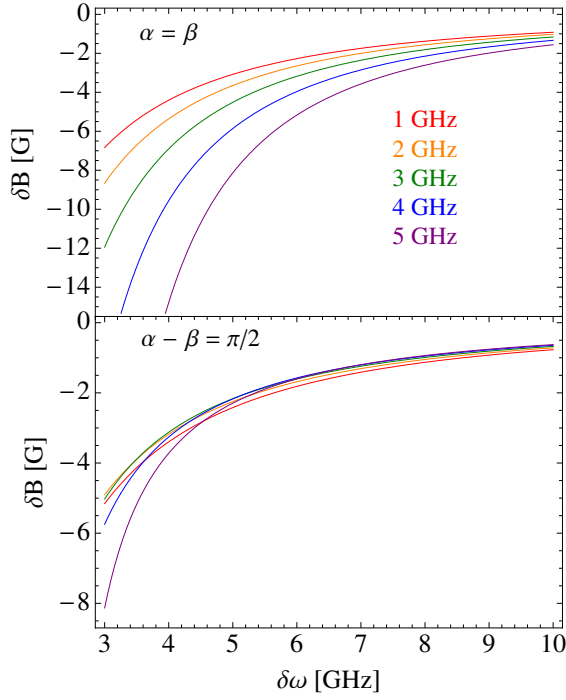


Figure 4. Pairs of required magnetic field variation δB and detuning $\delta\omega$ at fixed dipole coupling strength $\epsilon = 500$ MHz for different values of transversal strain $\delta_{\perp} = 1, 2, 3, 4$ and 5 GHz (from top to bottom) to fulfill the condition $\theta = \frac{\pi}{2}$ for precession around a rotation axis within the equatorial plane of the Bloch sphere for $\alpha = \beta = 0$.

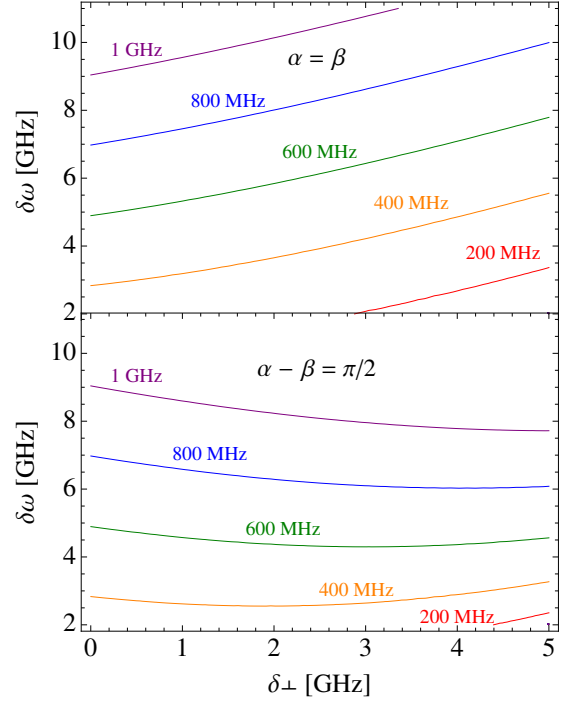


Figure 6. Pairs of detuning $\delta\omega$ and transversal strain δ_{\perp} that match the condition $\theta = \frac{\pi}{2}$ for precession around a rotation axis within the equatorial plane of the Bloch sphere for different dipole coupling $\epsilon = 100, 200, 400, 600, 800$ and 1000 MHz (from bottom to top) for $\alpha = \beta = 0$.

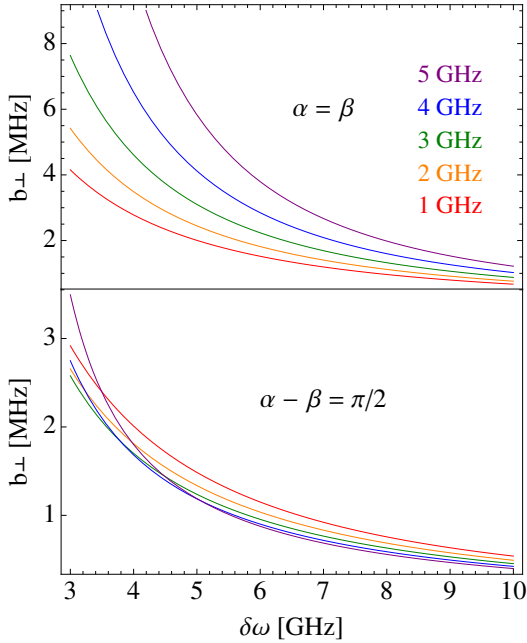


Figure 5. Precession frequency b_{\perp} for different values of transversal strain $\delta_{\perp} = 1, 2, 3, 4$ and 5 GHz (from left to right) for polarization parallel ($\alpha = \beta$) and perpendicular ($\alpha - \beta = \frac{\pi}{2}$) to strain with dipole coupling $\epsilon = 500$ MHz.

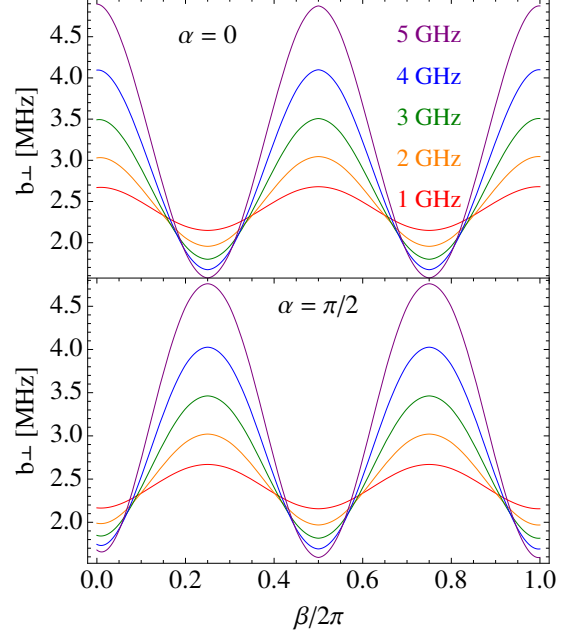


Figure 7. Precession frequency b_{\perp} around in-plane rotation axis at 10 GHz detuning for optical coupling $\epsilon = 500$ MHz and polarization in e_x ($\alpha = 0$) and e_y ($\alpha = \frac{\pi}{2}$) direction for different values of transversal strain $\delta_{\perp} = 1, 2, 3, 4, 5$ GHz (increasing amplitude) over strain direction angle β .

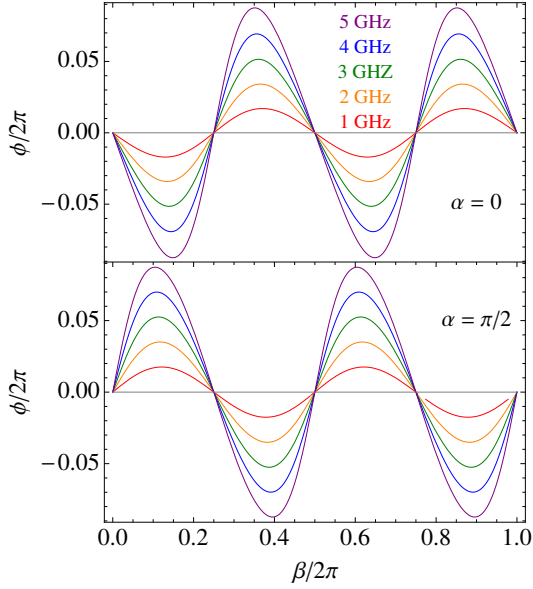


Figure 8. Non axial orientation angle ϕ of precession axis for polarization parallel ($\alpha = 0$) and perpendicular ($\alpha = \frac{\pi}{2}$) to e_x -orbitals symmetry axis in respect to strain orientation for different strengths of transversal strain.

splitting $g\mu_B\delta B$ with varying strain δ_\perp that fulfill the condition $\theta = \frac{\pi}{2}$ for an in-plane rotation axis. This defines an implicit function $\delta B(\delta\omega, \delta_\perp)$ given α and β , e.g. in the case of $\theta = \pi/2$ for $\alpha = \beta = 0$. To find the strength of spin-flip transitions, we substitute δB into the precession frequency for an in-plane rotation axis, b_\perp and plot it in Fig. 5 as a function of the optical frequency detuning $\delta\omega$ for different values of transversal strain. We find that the precession frequency b_\perp indeed increases with strain. Varying ϵ numerically shows that the precession frequency is still proportional to the intensity of the optical driving field $b_\perp|_{\theta=\frac{\pi}{2}} \propto \epsilon^2$. Note that the perturbative approach breaks down as detuning approaches strain (divergence of b_\perp in Fig. 5), restricted by the validity condition $\delta\omega \ll \delta_\perp$ for the Schrieffer-Wolff transformation in Eq. (4). We also investigate the dependence on the direction of strain and polarization (see Fig. 7). Expectedly we get the highest efficiency for collinear strain and polarization and a minimal efficiency for perpendicular relative orientation with an overall sinusoidal form of twofold symmetry. Changing the optical polarization angle α only leads to a uniform and continuous shift of this function (this has been checked for a variety of different values, but for simplicity we only show it for $\alpha = 0$ and $\alpha = \frac{\pi}{2}$). Thus, for weak strain, the resulting effective field only depends on the relative angle $\alpha - \beta$ between the strain and polarization angles. However, as the transversal strain δ_\perp increases beyond about 10 and 20 GHz, we start observing a modulation of the field with higher harmonics of $\alpha - \beta$. Numerical evaluation also reveals that the azimuthal angle (for in-plane orientation of the precession axis) is generally independent of optical coupling

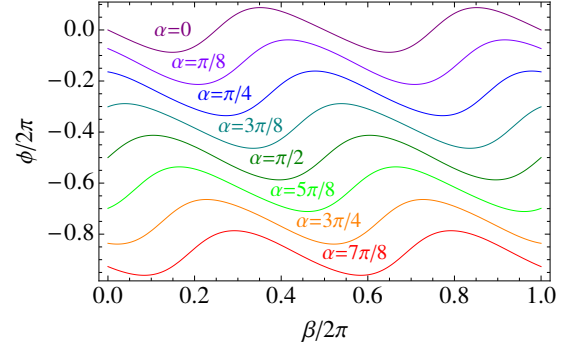


Figure 9. Non axial orientation angle ϕ of precession axis for different polarization angles α in respect to strain orientation at transversal strain $\delta_\perp = 5$ GHz.

strength and magnetic field,

$$\phi = \phi(\alpha, \beta, \delta_\perp, \delta\omega). \quad (21)$$

From Fig. 8 we see that for e_x/y -polarized light (i.e. $\alpha = 0, \frac{\pi}{2}$), the angle ϕ is well approximated by $\phi = \mp \hat{\phi}(\delta_\perp, \delta\omega)(\delta_\perp, \delta\omega) \sin 2\beta$ (at low strain), with an amplitude proportional to the intensity of the strain,

$$\hat{\phi} = \delta_\perp f(\delta\omega) \quad (22)$$

In Fig. 9, we show that the sinusoidal shape of ϕ as a function of α is slightly distorted for polarization angles $\alpha \neq n\frac{\pi}{2}$, $n \in \mathbb{N}$; we also find that this distortion grows with increasing strain.

C. High strain limit

In the high strain regime, the electronic states of the NV-center are energetically split into two orbital branches with largely separated energies E_x and E_y corresponding to a specific choice of coordinate axes, that fixes the orientation angle β . In this limit b_\perp and b_z (and thus the polar angle θ) become independent of the orientation angles of both strain and polarization. Expanding in δ_\perp^{-1} yields

$$b_\perp \simeq 2\Delta'' \frac{\epsilon^2}{\delta_\perp^2}, \quad (23)$$

and

$$\phi = 2(\alpha - 2\beta) - \frac{\pi}{2} + \mathcal{O}\left(\frac{1}{\delta_\perp}\right). \quad (24)$$

for the transversal part of the pseudo-field, and

$$b_z = -\frac{g\mu_B\delta B}{2} + 2(D_{\text{es}} - D_{\text{gs}}) \frac{\epsilon^2}{\delta_\perp^2} + \mathcal{O}\left(\frac{1}{\delta_\perp^3}\right), \quad (25)$$

for the longitudinal part. The higher orders contain higher harmonics, such as terms $\propto \Delta \cos 2(\alpha - 3\beta)$ for b_x and $\propto \Delta \sin 2(\alpha - 3\beta)$ for b_y in $\mathcal{O}\left(\frac{1}{\delta_\perp^3}\right)$, indicating strain induced third order transitions mediated by the $A_{1,2}$ levels.

V. CONCLUSION

We have shown that the effective precession axis and frequency of the ground state spin of the NV^- -center can be fully controlled by off-resonant optical excitation, by adjusting the frequency detuning $\delta\omega$ and linear polarization angle α of the optical driving field for a given intensity ϵ (optical dipole coupling) and magnetic field B . The orientation of the precession axis is determined by two angles θ and ϕ , where the first is depending on all parameters (including strain and polarization) and the latter is independent of magnetic field and optical coupling strength and basically controlled by polarization and strain. The strain effects can be compensated by external bias voltage³⁸. Since any unitary qubit operation (rotation around axis \mathbf{n} by angle γ) can be composed by successive rotations around two orthogonal axes on the Bloch sphere, a complete set of single-qubit operations can be generated optically in this way. From a purely geometric point of view, spin rotation about an axis within the equatorial plane of the Bloch sphere (where $b_z = 0$) is most effective for flipping the spin, although any axis other than the z -axis would do (the smaller the polar an-

gle θ , the more pulses are required). A full spin-flip is obtained by a $b_\perp \tau = \pi$ -rotation around an axis within the equatorial (x, y)-plane of the Bloch sphere, providing an estimate for the gate switching (optical pumping) time τ in the limit of large detuning and weak strain,

$$\tau \simeq \frac{\pi}{2} \frac{\delta\omega^2}{\Delta'' \epsilon^2}. \quad (26)$$

The switching time for spin-flip transitions is limited by the spin mixing term Δ'' , since the (above) condition implies via the off-resonant condition $\epsilon \ll \delta\omega$ the following lower limit for the spin-flip,

$$\tau \gtrsim \frac{\pi}{\Delta''} \approx 10 \text{ ns} \quad (27)$$

where for that latter estimate we assumed $\Delta'' = 0.2 \text{ GHz}$.

ACKNOWLEDGMENTS

We thank B. Buckley for discussions and F. Fehse for generating the graphics in Fig. 1 and the Konstanz Center for Applied Photonics (CAP) and BMBF QuHLRep for funding.

-
- ¹ R. Hanson and D. D. Awschalom, *Nature* **453**, 1043 (2008).
 - ² F. Jelezko, T. Gaebel, I. Popa, A. Gruber, J. Wrachtrup, *Phys. Rev. Lett.* **92**, 076401 (2004).
 - ³ T. A. Kennedy, J. S. Colton, J. E. Butler, R. C. Linares, and P. J. Doering, *Appl. Phys. Lett.* **83**, 4190 (2003).
 - ⁴ R. Hanson, O. Gywat, and D. D. Awschalom, *Phys. Rev. B* **74**, 161203(R) (2006).
 - ⁵ D. M. Toyli, D. J. Christle, A. Alkauskas, B. B. Buckley, C. G. Van de Walle, D. D. Awschalom, *arXiv:1201.4420* (2012).
 - ⁶ G. Balasubramanian *et al.*, *Nature Materials* **8**, 383 (2009).
 - ⁷ G. Davies and M.F. Hamer, *Proc. R. Soc. A*, **348**, 28 (1976).
 - ⁸ A. Gruber, A. Drabenstedt, C. Tietz, L. Fleury, J. Wrachtrup, and C. Borczyskowski, *Science* **276**, 2012 (1997).
 - ⁹ J. H. H. Loubser and J. A. van Wyk, *Diamond Res.* **1**, 11 (1977).
 - ¹⁰ J. Harrison, M. J. Sellars, N. B. Manson, *J. Lumin.* **107**, 245 (2004).
 - ¹¹ J. Harrison, M. J. Sellars, N. B. Manson, *Diamond Rel. Mater.* **15**, 586 (2006).
 - ¹² N. Manson, J. Harrison, M. Sellars, *Phys. Rev. B* **74**, 104303 (2006).
 - ¹³ M. H. Mikkelsen, J. Berezovsky, N. G. Stoltz, L. A. Col-dren, and D. D. Awschalom, *Nature Physics* **3**, 770 (2007).
 - ¹⁴ J. Berezovsky, M. H. Mikkelsen, N. G. Stoltz, L. A. Col-dren, D. D. Awschalom, *Science* **320**, 349 (2008).
 - ¹⁵ B. B. Buckley, G. D. Fuchs, L. C. Bassett, and D. D. Awschalom, *Science* **330**, 1212 (2010).
 - ¹⁶ E. Togan, Y. Chu, A. Imamoglu, and M. D. Lukin, *Nature* **478**, 497 (2011).
 - ¹⁷ C. Santori, P. Tamarat, P. Neumann *et al.*, *Phys. Rev. Lett.* **97**, 247401 (2006).
 - ¹⁸ X. F. He, N. Manson, P. Fisk, *Phys. Rev. B* **47**, 8809 (1993).
 - ¹⁹ A. Lenef, S. Rand, *Phys. Rev. B* **53**, 13441 (1996).
 - ²⁰ M. W. Doherty, N. B. Manson, P. Delaney, and L. C. L. Hollenberg, *New J. Phys.* **13**, 025019 (2011).
 - ²¹ J. R. Maze, A. Gali, E. Togan, Y. Chu, A. Trifonov, *New J. Phys.* **13**, 025025 (2011).
 - ²² E. van Oort, N. B. Manson, and M. Glasbeek, *J. Phys. C* **21**, 4385 (1988).
 - ²³ L. Rogers, M. McMurtie, M. Sellars *et al.*, *New J. Phys.* **11**, 063007 (2009).
 - ²⁴ P. Tamarat, N. Manson, J. Harrison *et al.*, *New J. Phys.* **10**, 045004 (2008).
 - ²⁵ A. Batalov, V. Jacques, F. Kaiser, P. Siyushev, P. Neumann, *Phys. Rev. Lett.* **102**, 195506 (2009).
 - ²⁶ G. D. Fuchs, V.V. Dobrovitski, R. Hanson, A. Batra, C. D. Weis, T. Schenkel, D. D. Awschalom, *Phys. Rev. Lett.* **101**, 117601 (2008).
 - ²⁷ P. Neumann, R. Kolesov, V. Jacques, J. Beck, J. Tisler, *New J. Phys.* **11**, 013017 (2009).
 - ²⁸ P. Hemmer, R. Turukhin, A. V. Shahriar, M. S. Musser, J. A., *Opt. Lett.* **26**, 361 (2001).
 - ²⁹ J. Schrieffer and P. Wolff, *Phys. Rev.* **149**, 491 (1966).
 - ³⁰ This can be justified by a second Schrieffer-Wolff transformation.
 - ³¹ R. Hanson, F. Mendoza, R. Epstein, D. Awschalom, *Phys. Rev. Lett.* **97**, 087601 (2006).

- ³² F. Jelezko, I. Popa, A. Gruber, C. Tietz, J. Wrachtrup, Appl. Phys. Lett. **81**, 2160 (2002).
- ³³ A. Gali, M. Fyta, E. Kaxiras, Phys. Rev. B **77**, 155206 (2008).
- ³⁴ N. B. Manson, J. P. Harrison, and M. J. Sellars, arXiv:cond-mat/ 0601360 (2006).
- ³⁵ A. Lenef and S. Brown, D. Redman, S. Rand, J. Shigley, E. Fritsch, Phys. Rev. B **53**, 13427 (1996).
- ³⁶ L. Robledo, H. Bernien, I. van Weperen, R. Hanson, Phys. Rev. Lett. **105**, 177403 (2010).
- ³⁷ P. Tamarat, T. Gaebel, J. Rabeau, M. Khan, A. Greentree, Phys. Rev. Lett. **97**, 083002 (2006).
- ³⁸ L. C. Bassett, F. J. Heremans, C. G. Yale, B. B. Buckley, and D. D. Awschalom, Phys. Rev. Lett. **107**, 266403 (2011).